Progress In Electromagnetics Research, PIER 9, 289–310, 1994

MODELING OF HELIX-LOADED CHIRAL RADAR-ABSORBING LAYERS

C. R. Brewitt-Taylor

1. Introduction

There are a number of recent papers suggesting that chiral materials might provide a useful additional degree of freedom in the design of radar absorbing materials [1–4]; for example Varadan et al. [1] show apparently useful results such as greater bandwidth. These initial investigations allow arbitrary chiral parameter to be used, and leave unanswered the questions of what chirality is achievable in practice, and whether any undesirable side-effects are introduced at the same time.

The purpose of the present paper is to investigate the usefulness of chiral media as a radar absorbing material, taking into account the limitations imposed by practically feasible chirality. To do this, we

consider the case of medium loaded with wire helices, as have been used in published experimental work; it is also relevant to chiral polymers which work by providing a helical conducting path. An analysis of such an absorber is constructed, starting from the geometry of the helices, and proceeding via their computed polarizabilities to the effective dielectric, magnetic and chiral constants of a composite medium, and finally to the reflection coefficient from a layer of the medium. This procedure is then used in a optimization loop, to find what can be achieved with helix-loaded mixtures in the way of broad-band absorbers, compared to simpler media.

Calculations of the chirality of a material from the microscopic properties of the chiral particles have been previously performed for a one-turn helix-cum-dipole [5], and for a helical string of polarizable particles [6]. Reports of experimental results are now starting to appear. Measurements have been made for planar slabs in reflection and transmission [7–9]; and in circular waveguides [10]. So far the interpretation of the results in terms of chiral electromagnetic theory is only qualitative, without detailed numerical comparisons.

2. Elementary Theory

2.1 Constitutive Relations

There are several different constitutive relations for chiral media used in the literature [11,12]. For time-harmonic fields the different relationships are mutually convertible, and in this sense none is more fundamental than another. The set used here has been chosen on the ground of convenience only, like the choice of coordinate system for a mechanical problem:

$$\begin{aligned} \mathbf{D} &= \epsilon \mathbf{E} - i\chi \mathbf{H}, \\ \mathbf{B} &= i\chi \mathbf{E} + \mu \mathbf{H}. \end{aligned} \tag{1}$$

The parameter χ represents the magnetic polarization induced by an electric field $\mathbf{E}$, which turns out by reciprocity to equal the electric polarization induced by a magnetic field $\mathbf{H}$. The use of the symbol χ for the chirality parameter has obvious mnemonic value. The factor i is introduced so that a pure real chirality describes a lossless medium, like pure real permittivity and permeability. This set of relations turns

out to give a particularly simple form to the analysis of plane waves, and it fits conveniently with the calculation of the polarizabilities of helices as done below. It is similar to the set used by A.H.Sihvola and others [12,13].

Another commonly used set of constitutive relations is that of the Varadans and Lakhtakia, with chiral parameter β (e.g. [1,11]):

$$\begin{aligned} \mathbf{D} &= \epsilon(\mathbf{E} + \beta \operatorname{curl} \mathbf{E}), \\ \mathbf{B} &= \mu(\mathbf{H} + \beta \operatorname{curl} \mathbf{H}). \end{aligned} \tag{2}$$

The translation between one set and another can easily be found. With an $e^{i\omega t}$ time variation we find (compare [12]):

$$\begin{aligned} \epsilon &= \epsilon_V/(1 - k_V^2\beta^2), \\ \mu &= \mu_V/(1 - k_V^2\beta^2), \\ \chi &= -\omega\mu_V\epsilon_V\beta/(1 - k_V^2\beta^2), \end{aligned} \tag{3}$$

with $k_V^2 = \omega^2\epsilon_V\mu_V$, where ϵ_V and μ_V refer to these parameters as defined by Varadan et al., in contrast to our definitions without subscript. We notice that the different definition of chirality affects also the ordinary permittivity and permeability. If the chirality is small ($k_V^2\beta^2 \ll 1$), then the two definitions of ϵ and μ are approximately the same, and the definitions of chirality differ only by a constant factor. But for larger chirality differences of order χ^2 appear. An effect attributed to changing the chirality in one description may be attributed to the associated change of ϵ or μ in another description.

2.2 Chiral Plane Waves

The properties of plane waves in chiral media are found by looking for solutions of Maxwell's equations with the chiral constitutive relations, in the form of plane waves in the z-direction, with the usual $\exp[i(\omega t - pz)]$ variation. Substituting these into Maxwell's curl-equations, we find that there are four possible values of the propagation constant p, which with our constitutive relations are simply: $p = \pm k \pm \omega\chi$, where $k = \omega\sqrt{(\mu\epsilon)}$. Of these solutions, $p = k \pm \omega\chi$ represents waves traveling upwards in z (for reasonably small chirality), and $p = -k \pm \omega\chi$ represent waves traveling downwards in z. We also notice that χ cannot have an imaginary part if k is real; for if it did,

one of the upward waves would be a growing wave, which is not possible. Thus any loss mechanism in the chirality must be associated with loss in ϵ or μ to prevent this. This is an illustration that arbitrary chirality is not necessarily possible. For each possible wavenumber, we can find the corresponding field components; the results are in the form of circularly polarized waves, with $E_y = \pm iE_x$, and wave impedance $E_x/H_y = -E_y/H_x = \sqrt{(\mu/\epsilon)}$. Thus we find that for these constitutive relations we have the particularly simple results that (a) the change in propagation constant is linearly proportional to the chirality, and (b) the expression for the wave impedance does not contain the chirality.

2.3 Reflection from Chiral Slab Absorber

With our interest in radar absorbing materials, we now proceed to consider the reflection from a chiral slab absorber on a metal backplane at normal incidence. Let the slab have thickness d and properties ϵ, μ and χ. The wave will be incident from free space (ϵ_0, μ_0). The fields in the air are expressed by an incident linearly polarized field of unit magnitude, and reflected co- and cross-polarized fields R_1 and R_2 respectively. The fields in the slab will be expressed as a sum over the four circular polarized modes (two traveling up and two traveling down). The boundary conditions connecting the various waves are (i) that the tangential electric field is zero on the metal backplane, and (ii) that the tangential electric and magnetic field components are continuous across the slab-air interface. We have six unknowns and six equations, so we can find the reflection coefficients. The procedure is similar to that of [1], though they did not solve for the reflection coefficients algebraically, but solve the equations numerically.

The solution can be carried out algebraically, and it is:

$$\begin{aligned} R_1 &= \frac{Z + iZ_0 \cot(kd)}{Z - iZ_0 \cot(kd)}, \\ R_2 &= 0. \end{aligned} \tag{4}$$

Here $Z = \sqrt{(\mu/\epsilon)}$ is the wave impedance in the slab, and Z_0 is the wave impedance in free-space.

We notice first that the cross-polar reflection R_2 is zero. It can be shown that there can be no cross-polar return from the principle of reciprocity. From the point of view of radar absorption, this result means that the slab does not "lose" part of an incident radar signal by

reflecting it into the other polarization where it might not be picked up.

Turning to the co-polar reflection coefficient, we find that it is exactly the same result as for a non-chiral slab with the same ϵ and μ: this point is also noted by Tretyakov et al. [14]. It can be understood by noting that with our constitutive relations the chirality neither affects the impedance of the waves, nor does it affect the total down-and-up phase of the circular waves in the slab, since the slowing in one direction cancels the speed-up in the other. This result seems a discouragement for the possibility of using chiral media to make an improved radar absorber. It is also apparently contradicted by the numerical results for this problem given in [1]. This strikingly illustrates the apparent paradox that can arise because of the different forms of constitutive relations. Varadan's chirality, when converted to our description Eq. (3) increases the permeability and permittivity considerably (since the denominator $(1 - k_V^2 \beta^2)$ approaches zero in some of his cases), and so improves the reflection coefficient. We have reproduced some of his results by converting to our description and then using the reflection coefficient formula (4) just obtained.

Away from normal incidence the chirality does appear explicitly in the co-polar reflection coefficient, and the cross-polar reflection is non-zero.

3. Microscopic Analysis of Chiral Media

Most practical chiral media are composites containing chiral objects in a non-chiral host medium. The chiral objects will in general affect all the electromagnetic parameters ϵ, μ, and χ. This leads us to go behind the constitutive relations, and carry out a microscopic analysis of a composite chiral medium. The composite chosen consists of resistive wire helices in a uniform isotropic dielectric host medium. The method-of-moments computer program NEC [15] is used to carry out a microscopic analysis of a single inclusion. We then calculate the effective medium parameters of a composite material containing such helices, and compute the reflection from a single layer chiral absorber made of such a material. In this way we see the total effect of the helices. The treatment is quasi-static, in that we proceed via dipole polarizabilities only. It is assumed that the composite medium can be

represented by a homogeneous effective medium: in practice a composite medium will show residual differences from this theory due to its microscopic inhomogeneity and the finite number of scatterers.

3.1 Extraction of Polarizabilities

The computer program NEC can compute the current distribution in a given wire structure, in response to any incident plane wave. Once the current has been computed, a separate computer program is used to compute the electric moment $\mathbf{p_e}$ and magnetic moment $\mathbf{p_m}$ by numerical integration. The moments are:

$$\begin{aligned} \mathbf{p_e} &= \frac{1}{i\omega} \int \mathbf{I}\, dl, \\ \mathbf{p_m} &= \frac{1}{2} \int I\mathbf{r} \times d\mathbf{r}. \end{aligned} \tag{5}$$

Here $\mathbf{r}$ is the vector from an origin to an element of the current, and $\mathbf{dr}$ is the vector element of length pointing along the wire; $\mathbf{I}$ is the current in the wire and I its magnitude; and ω is the angular frequency.

A general object has both electric and magnetic polarizabilities simultaneously, and is likely also to be anisotropic. Since an incident plane wave contains both electric and magnetic fields together, we will often excite more than polarizability at once, and this raises the problem of sorting out the individual polarizability components from the results.

There are in general 4 complex polarizability tensors, relating the induced electric and magnetic moments to the incident electric and magnetic fields.

$$\begin{aligned} \mathbf{p_e} &= \alpha_{ee}\epsilon_0 \mathbf{E} + \alpha_{em}\epsilon_0 Z_0 \mathbf{H}, \\ \mathbf{p_m} &= \alpha_{me}\mathbf{E}/Z_0 + \alpha_{mm}\mathbf{H}. \end{aligned} \tag{6}$$

Here α_{ee} is the usual electric polarizability, and α_{mm} is the usual magnetic polarizability; these both have dimensions of volume. There are two cross-polarizabilities α_{em} and α_{me}, which we have defined with factors of ϵ_0 and Z_0 (the impedance of free-space) introduced to give all the polarizabilities the same dimensions of volume.

These four 3×3 tensors have 36 components between them. We can apply six different incident plane waves to the object (up and down

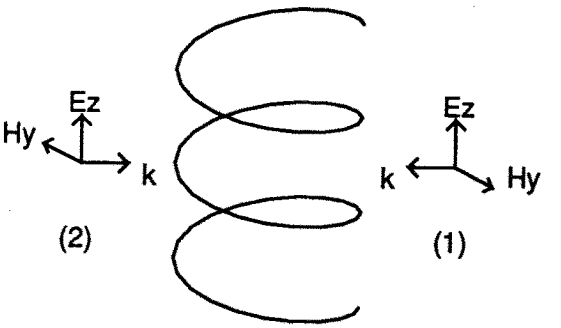

Figure 1. Incident waves for extraction of polarizabilities. (Add (1) + (2) gives E_z effect, subtract (1)-(2) gives H_y effect.)

each of the three axes), with two polarizations each. For each incident wave we can compute the three components each of $\mathbf{p_e}$ and $\mathbf{p_m}$. Thus there are 72 complex values available, which is more than enough to find the 36 polarizability components. We use three pairs of oppositely directed waves (Figure 1), and find the effects of the separate fields by adding and subtracting the dipole moments obtained with each of the pairs. For example, in Figure 1, adding the results of waves 1 and 2 will yield the effects of E_x, namely the three electric polarizabilities $(\alpha_{ee})_{ix}$ and the three cross-polarizabilities $(\alpha_{me})_{ix}$ (for $i = x, y, z$), with the effect of H_y canceling out. Subtracting this pair cancels the E_x effect and yields the H_y effects, namely the magnetic polarizabilities $(\alpha_{mm})_{iy}$ and the cross-polarizabilities $(\alpha_{em})_{iy}$. Similar adding and subtracting for the other two pairs, obtained by cyclic permutation of x, y, and z, yields all the 36 polarizabilities, and we can thus deal with any case of anisotropy or chirality. These polarizabilities are frequency-dependent, so the above procedure is carried out at each frequency of interest.

Having obtained the tensor polarizabilities, we average the diagonal components to obtain the (scalar) polarizabilities of a randomly oriented collection of particles, and discard the off-diagonal components, which will average to zero.

The NEC program used to analyze the particles assumes that the host medium is air, whereas in our problem it might be a dielectric medium. This prevents us from using a lossy host medium, and so requires us to make the wires resistive to provide a loss mechanism. The different real dielectric constant can be handled by scaling the problem. Any metal wire object in the host medium is equivalent to the same object in air operating at higher frequency (to maintain the same wavelength in the medium) and with higher resistance (to maintain the same ratio to the wave impedance of the medium). The scaling factor is $\sqrt{\epsilon_r}$ for both frequency and resistance. The resulting polarizabilities are "relative to the medium", i.e. the formulae for computing the effective composite medium parameters are unchanged except that we must write the host medium actual permittivity $\epsilon_r\epsilon_0$ instead of ϵ_0 wherever it appears. In practice there may equally well be loss in the host medium, instead of or as well as in the helices; an analysis on similar lines might be performed for this case, but has not been done here.

3.2 Effective Medium Parameters

In this section we proceed from the particle polarizabilities α_{ee}, α_{mm}, α_{em} and α_{me}, which have been computed by microscopic analysis of a single particle, to the effective permittivity, permeability, and chirality of the composite medium. The treatment is adapted from that given in [13] for spherical chiral particles, which is a generalization of the usual Clausius-Mossotti derivation for the dielectric constant of composite media.

If $\mathbf{p}$ and $\mathbf{m}$ are the electric and magnetic polarizations per unit volume, we have with the usual definitions:

$$\begin{aligned} \mathbf{D} &= \epsilon_0\mathbf{E} + \mathbf{p}, \\ \mathbf{B} &= \mu_0(\mathbf{H} + \mathbf{m}). \end{aligned} \tag{7}$$

The polarizations are given by the sums of the averaged microscopic polarizabilities multiplied by the number of particles per unit volume n, as follows:

$$\begin{aligned} \mathbf{p} &= n\alpha_{ee}\epsilon_0\mathbf{E}_L + n\epsilon_0\alpha_{em}\mathbf{H}_L Z_0, \\ \mathbf{m} &= n\alpha_{mm}\mathbf{H}_L + n\alpha_{me}\mathbf{E}_L/Z_0. \end{aligned} \tag{8}$$

Here $\mathbf{E}_L$ and $\mathbf{H}_L$ are the local fields at the particles, which are different from the applied fields $\mathbf{E}$ and $\mathbf{H}$ by the contributions from the surrounding polarization. We assume that this contribution is given by the usual Clausius-Mossotti formula:

$$\begin{aligned} \mathbf{E}_L &= \mathbf{E} + \mathbf{p}/(3\epsilon_0), \\ \mathbf{H}_L &= \mathbf{H} + \mathbf{m}/3. \end{aligned} \tag{9}$$

Eliminating the polarizations $\mathbf{p}$ and $\mathbf{m}$ from these equations with the help of Eq. 7, we obtain expressions for the local fields:

$$\begin{aligned} \mathbf{E}_L &= \frac{\mathbf{D} + 2\epsilon_0 \mathbf{E}}{3\epsilon_0}, \\ \mathbf{H}_L &= \frac{\mathbf{B} + 2\mu_0 \mathbf{H}}{3\mu_0}. \end{aligned} \tag{10}$$

These expressions can then be substituted into the expressions for the polarizations (Eq. 8), and these in turn can be substituted into Eq. 7. The resulting equations are then solved for $\mathbf{D}$ and $\mathbf{B}$ in terms of $\mathbf{E}$ and $\mathbf{H}$, and cast in the same form as the constitutive relations (1). Equating coefficients in the two pairs of equations gives the properties of the composite medium:

$$\begin{aligned} \epsilon &= \frac{\epsilon_0(1 + 2n\alpha_{ee}/3)(1 - n\alpha_{mm}/3) + 2n^2\alpha_{em}\alpha_{me}/9}{(1 - n\alpha_{ee}/3)(1 - n\alpha_{mm}/3) - n^2\alpha_{em}\alpha_{me}/9}, \\ \mu &= \frac{\mu_0(1 + 2n\alpha_{mm}/3)(1 - n\alpha_{ee}/3) + 2n^2\alpha_{em}\alpha_{me}/9}{(1 - n\alpha_{ee}/3)(1 - n\alpha_{mm}/3) - n^2\alpha_{em}\alpha_{me}/9}, \\ \chi &= \frac{in\alpha_{em}\sqrt{\epsilon_0\mu_0}}{(1 - n\alpha_{ee}/3)(1 - n\alpha_{mm}/3) - n^2\alpha_{em}\alpha_{me}/9}. \end{aligned} \tag{11}$$

These properties are frequency-dependent, through the underlying microscopic polarizabilities. The two values of χ obtainable from $\mathbf{D}$ in terms of $\mathbf{H}$ and from $\mathbf{B}$ in terms of $\mathbf{E}$ are the same, providing $\alpha_{em} = -\alpha_{me}$, as it should be by reciprocity.

If there is no chirality, the formulae reduce to the usual Clausius Mossotti formula. For small particle densities (only terms linear in n), the formulae reduce to the expected forms:

$$\begin{aligned} \epsilon &= \epsilon_0(1 + n\alpha_{ee}), \\ \mu &= \mu_0(1 + n\alpha_{mm}), \\ \chi &= in\alpha_{em}\sqrt{\epsilon_0\mu_0}. \end{aligned} \tag{12}$$

But if there is chirality and the particle density are not very small, we see that each composite medium property involves all of the microscopic polarizabilities. Also the reflection coefficient (Eq. 4) depends indirectly on all the polarizabilities. A consequence of this is that a one-handed chiral mixture would differ from a racemic mixture (equal numbers of each hand) of the same particles not only in the chirality, but also in the permittivity and permeability. However this effect depends on the square of the cross-polarizability, and so would be small where the chirality is small.

3.3 Summary of Procedure

We now have a complete method to predict the reflection from a composite medium from the microscopic properties of the included particles. We require as input the thickness and dielectric constant of the host medium, and the geometry and resistance of the inclusions. The process is then as follows:

(a) Scale the frequency and the resistance of the inclusions by the square root of the host dielectric constant.
(b) Write a NEC input file describing an included particle, the six incident waves discussed in Section 3.1 with unit electric field magnitude, and the desired frequencies.
(c) Run NEC, read the currents in the included particles from its output file, and integrate over these currents to obtain the induced electric and magnetic moments using Eq. 5.
(d) Take sums and differences of the moments in the pairs of incident waves, to obtain the moments with single electric or magnetic field excitations; and divide by the incident fields ($E = 1$ and $H = 1/Z_0$) to obtain the polarizability tensors.
(e) Average the diagonal tensor components to obtain the polarizabilities of a randomly oriented composite.
(f) From the polarizabilities, the number of particles per unit volume,

and the host dielectric constant, obtain the composite medium effective parameters using Eq. 11.
(g) From the composite medium properties and the thickness, calculate the reflection coefficient using Eq. 4.

4. Properties of Single Helices

As an initial exploration, the moments of a number of single-turn helices in free space were computed. The cylinder length and loop radius were adjusted together to keep the wire length constant, so that the variation corresponded to progressively flattening the same wire loop. Just one intermediate example is shown in Figure 2. The polarizabilities shown are averages over the three axial directions, corresponding to a mixture with random spiral orientations. There are electric and magnetic polarizabilities, and there are also the cross-polarizabilities which give rise to chirality. In the bottom section of Figure 2 is shown both cross-polarizabilties α_{em} and α_{me}, marked by circles and crosses. We see that they roughly obey the reciprocity requirement $\alpha_{em} = -\alpha_{me}$. All the polarizabilities show a resonant form of frequency dependence.

Figure 3 shows the resonant frequency (in the form of the ratio of wire length to wavelength) as a function of the spiral cylinder length. The frequency is nearly constant at $L = 0.45\lambda$ for the 1-turn spiral, with variation up to $L = 0.5\lambda$ for 2 turns, and still more variation to $L = 0.6\lambda$ for 4 turns. This is similar to the value of $L/\lambda = 0.5$ reported in early experimental work [16–18].

In Figure 4 is plotted the variation of the maximum magnitude (as the frequency is varied) of the averaged polarizabilities as a function of the helix cylinder length. The electric polarizability reduces steadily from its value for a dipole towards the smaller value for a flat loop (not zero because of the polarizability in the plane of the loop). The magnetic polarizability increases steadily from zero for a dipole to a maximum value for a flat loop, as the loop radius increases. The cross-polarizability increases from zero for a dipole, to a maximum when the aspect ratio is around 1, and then decrease back to zero for a flat loop.

A simple model of the polarizabilities of a helix can be constructed, guided by the above computations, which illuminates some

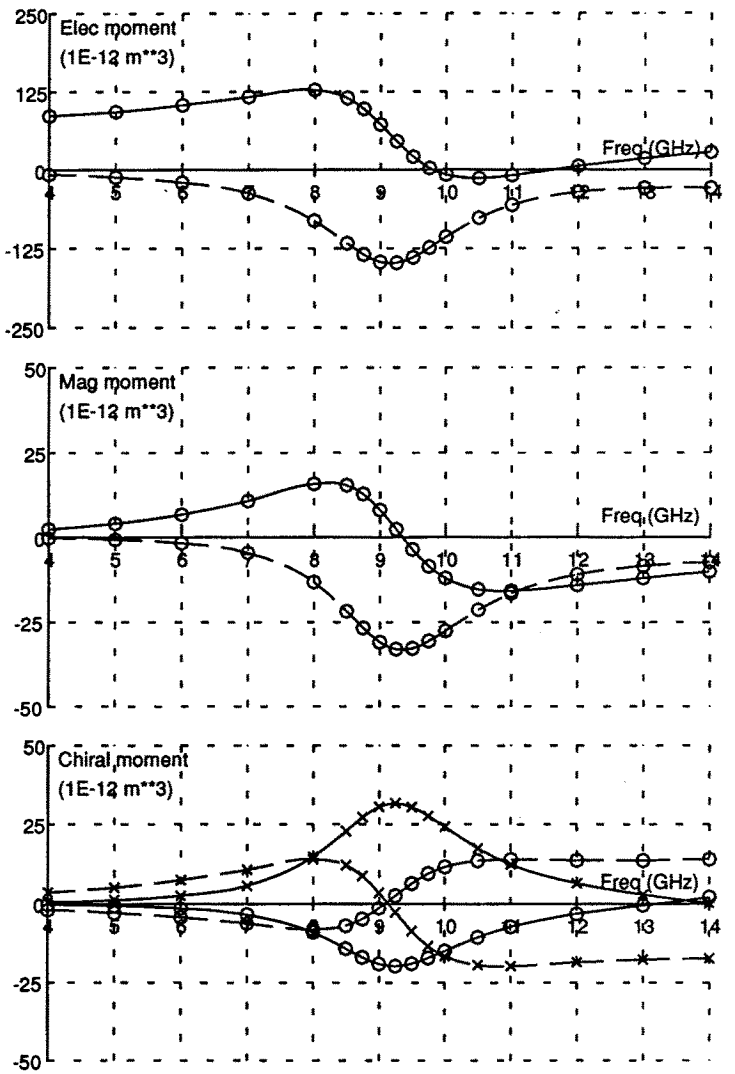

Figure 2. Averaged moments of 1 turn helix in air. (Radius 2.19 mm, cyl. length 6 mm, wire length 15 mm, wire radius 0.1 mm, end-to-end resistance 150 Ohm; full= real part, broken = image part.)

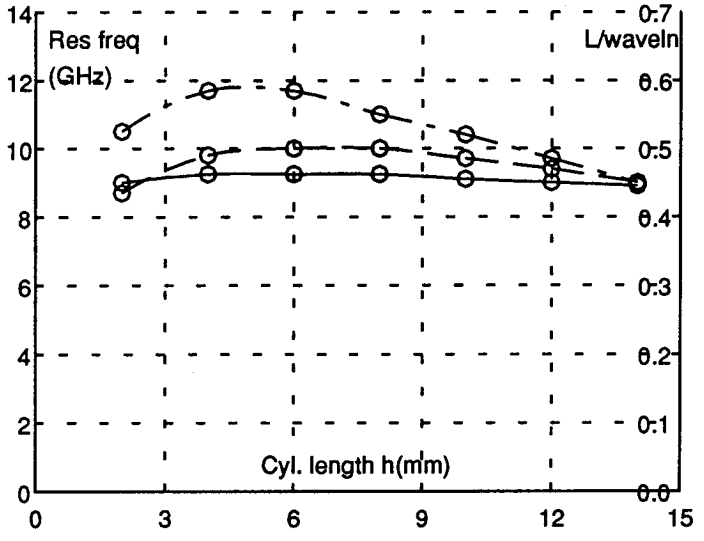

Figure 3 Resonant frequency of Helices. (Turns: full=1, broken = 2, chain = 4.)

aspects of the behavior of helices as chiral inclusions. Consider an N-turn helix of cylinder radius r, oriented with the cylinder length along the z-axis. Let the wire be inclined at an angle θ to the transverse $(x-y)$ plane: then $\theta = 90°$ gives the special case of a straight wire, and $\theta = 0$ gives a flat loop. The cylinder length of the helix is then $h = 2\pi N r \tan\theta$, and the length of the wire is $L = 2\pi N r/\cos\theta$.

Consider first excitation by an electric field E_z along the cylinder length. This will induce a voltage hE_z along the wire. The current flowing is then $I = hE_z/Z_A$, where Z_A is the impedance of the wire treated as an antenna. This impedance will have a resonant form, which can be approximated over some frequency band by a suitable R-L-C circuit. For the present purpose we shall not need an explicit form for Z_A. But we will assume that it is independent of the tightness of the spiral (angle θ). This assumption is motivated by the observation that the resonant frequency is approximately constant with θ for fixed wire

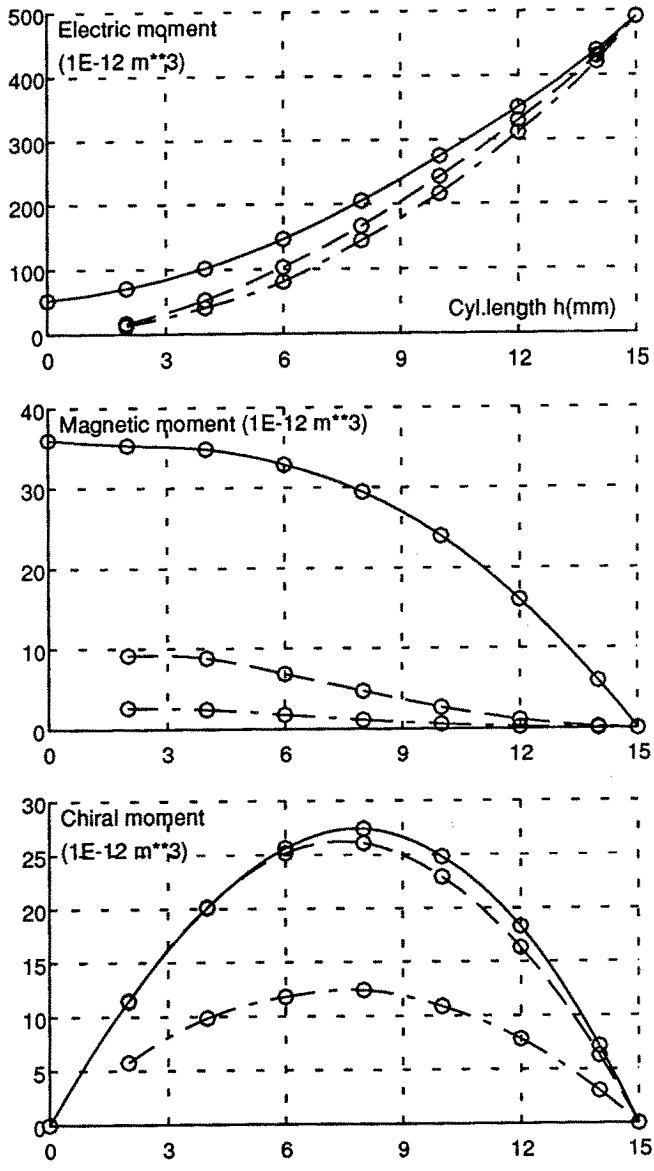

Figure 4. Moments of resonant helices. (Turns: full = 1, chain = 4)

length. The induced current gives an electric dipole moment:

$$p_e = \frac{1}{i\omega}\int I dz = \frac{Ih}{i\omega} = \frac{E_z h^2}{i\omega Z_A}. \tag{13}$$

The electric polarizability is then:

$$\alpha_{zz} = \frac{p_e}{\epsilon_0 E_z} = \frac{h^2}{i\omega\epsilon_0 Z_A}. \tag{14}$$

This predicts that the electric polarizability will increase with the square of the cylinder length h, which is approximately obeyed in Figure 4, especially for the multi-turn spiral where x and y-moments are smaller. The current flowing around the wire also produces a magnetic moment:

$$p_m = \frac{1}{2}\int I\mathbf{r}\times d\mathbf{r} = \pi N I r^2 = \frac{\pi N E_z h r^2}{Z_A}. \tag{15}$$

The chiral-polarizability is then:

$$(\alpha_{me})_{zz} = \frac{p_m Z_0}{E_z} = \frac{\pi N h r^2 Z_0}{Z_A}. \tag{16}$$

Consider next a magnetic excitation. A magnetic field H_z induces a voltage proportional to the flux enclosed: $V = -N\pi r^2 \cdot i\omega\mu_0 H_z$. The induced current is given by dividing by the impedance, as before: $I = -N\pi r^2 i\omega\mu_0 H_z/Z_A$. The corresponding magnetic moment is:

$$p_m = \pi N I r^2 = -\frac{N^2\pi^2 r^4 i\omega\mu_0 H_z}{Z_A}, \tag{17}$$

and the magnetic polarizability is

$$(\alpha_{mm})_{zz} = \frac{p_m}{H_z} = -\frac{i\omega\mu_0 N^2\pi^2 r^4}{Z_A}. \tag{18}$$

This current flowing along the length of the spiral gives an electric moment:

$$p_e = \frac{Ih}{i\omega} = -\frac{N\pi r^2 h\mu_0 H_z}{Z_A}, \tag{19}$$

and the chiral polarizability is:

$$(\alpha_{em})_{zz} = \frac{p_e}{\epsilon_0 Z_0 H_z} = -\frac{N\pi r^2 h Z_0}{Z_A}. \tag{20}$$

We see that this obeys the reciprocity relation $\alpha_{em} = -\alpha_{me}$.

We can now find the maximum available chiral polarizability. We will restrict attention to the half-wavelength resonance, and assume that this occurs when the wire length L is exactly half a wavelength. This condition is $2N\pi r/\cos\theta = \lambda/2$, which can be written $r = \cos\theta/(2Nk)$, with k being the wavenumber. In the expression for the chiral polarizability, we first substitute for h using the value at the head of this section, and then substitute for r using the half-wavelength condition; the result is

$$(\alpha_{me})_{zz} = \frac{\pi^2 Z_0}{4k^3 Z_A} \frac{\cos^2\theta \sin\theta}{N}. \tag{21}$$

This results clearly goes to zero at $\theta = 0$ and $\theta = 90°$, as shown in Figure 4, and as expected since these extreme cases are non-chiral. It has a maximum value at angle $\theta = \tan^{-1}(1/\sqrt{2}) \approx 35°$. This makes the ratio of the pitch to the wire length in each turn $\sin\theta = 0.57$, which is near the value of 0.55 given in [6] for interacting dipoles. This is also the value of the ratio h/L, so that in our computations, the maximum chirality should occur at cylinder length $h = 0.55 \times 15 \approx 8$ mm, independent of the number of turns. This agrees with the detailed calculations (Figure 4). We should notice that this is a fairly elongated spiral: the turns are not close together.

The simple theory also predicts that the maximum chirality should be inversely proportional to the number of turns N. This is observed in the Figure 3 between the 2-turn and 4-turn spiral, but not for the 1-turn spiral. Now the polarizabilities plotted in this figure are the averages for the three axes, appropriate to a randomly oriented mixture. Inspection of the separate polarizabilities shows that for $N \geq 2$ the z-directed chiral polarizability is the only significant one, whereas for $N = 1$ there is also a negative y-directed chiral polarizability, which partially cancels the z-polarizability in the average, giving a smaller average chiral polarizability than might be expected.

It is noticeable in Figure 4 that the electric polarizabilities are considerably greater than the magnetic and chiral moments, by a factor of at least 4 at the maximum chiral moment ($h = 8$ mm). Since we have

defined the polarizabilities with the same dimensions, these magnitudes are physically significant. Using the above formulae, we find that the ratio of the magnitudes is:

$$\frac{|\alpha_{me}|}{|\alpha_{ee}|} = \frac{\cos^2\theta}{4N\sin\theta} \approx \frac{0.29}{N} \tag{22}$$

at the maximum chiral moment. This is in rough agreement with the computations. If this associated large electric moment is a nuisance, it may be preferable to operate with flatter spiral, where the ratio α_{me}/α_{ee} is larger: a moderate flattening reduces the chiral moment only a little, whereas the electric moment is considerably smaller. The ratio α_{me}/α_{ee} does not have a maximum: it increases monotonically as the spiral is flattened, but very flat loops have both moments small and so are less useful.

5. Absorber Optimizations

As well as direct calculations by the above procedure, we have also used the procedure within an optimization loop to design optimized helix-loaded composites. For a general helix mixture there are six adjustable parameters, which are the host dielectric constant, the number of helices per unit volume, and the helix cylinder length, loop radius, number of turns, and resistance. The hand of the spiral chirality can be changed by making the cylinder length negative. If the loop radius is set to zero, the spiral reduces to a straight dipole (and the number of turns is irrelevant). If the cylinder length is zero and there is just less than one turn, the spiral reduces to a flat broken loop. These limiting cases are both non-chiral, and provide a basis of comparison for the general chiral helix mixtures. In all optimizations the layer thickness is held constant; in the results reported below it was 3 mm. The method of optimization chosen is to minimize the sum of the power reflection coefficients over a set of frequencies covering the desired frequency band, by adjusting some or all of the parameters listed above.

A number of optimizations were carried out varying all six parameters. These are very time-consuming, as might be expected. It was found that these did not improve the reflection curve significantly, and they often made little change to some of the parameters. This

	Host ϵ	N (m^{-3})	R (Ω)	L (mm)	r (mm)
Dipole	11.1	1.6×10^8	68	4.91	0
$L/2r = 2$	7.5	4.8×10^8	97	2.16	0.54
$L/2r = 1$	5.7	9.3×10^8	92	1.10	0.55
$L/2r = 1/8$	1.4	2.1×10^9	127	0.13	0.54

Table 1. Optimized helix-loaded layers.

suggests that the extra degrees of freedom do not immediately allow an increase of bandwidth, but suggests instead that the extra freedom is redundant. Instead of pursuing six-parameter optimizations, it was decided to fix two of the parameters, and try a series of four-parameter optimizations. In these runs, the parameters held fixed are the number of turns, and the aspect ratio of the spiral (the ratio of its cylinder length to its diameter). Optimizations have been performed for spiral of various aspect ratios, with one, two, and four turns. The reflection coefficients for two-turn spiral are plotted in Figure 5; dimensions of the optimized helices are given in Table 1. Reflection curves for different numbers of turns are qualitatively similar.

The reflection curve for a dipole (marked with plus-signs Figure 5) is similar in general shape to that for a flat loop (crosses), but the dipole has the lower frequency notch deeper, and the loop has the upper notch deeper. This two-notch shape is a consequence of the frequency dependence of the effective dielectric constant, due to the frequency dependent polarizabilities of the helices. This shape can also be obtained with straight wires; it is not an effect of the chirality. The various intermediate chiral cases have intermediate forms of reflection coefficients, with the two notches more equal in depth. The various aspect ratio and number of turns of the helices, and the associated chirality, do not give any significant advantage.

It is found that the number of spiral per unit volume is least for straight dipoles, presumably because the electric moments are largest for dipoles. Thus straight dipoles appear as the most efficient means

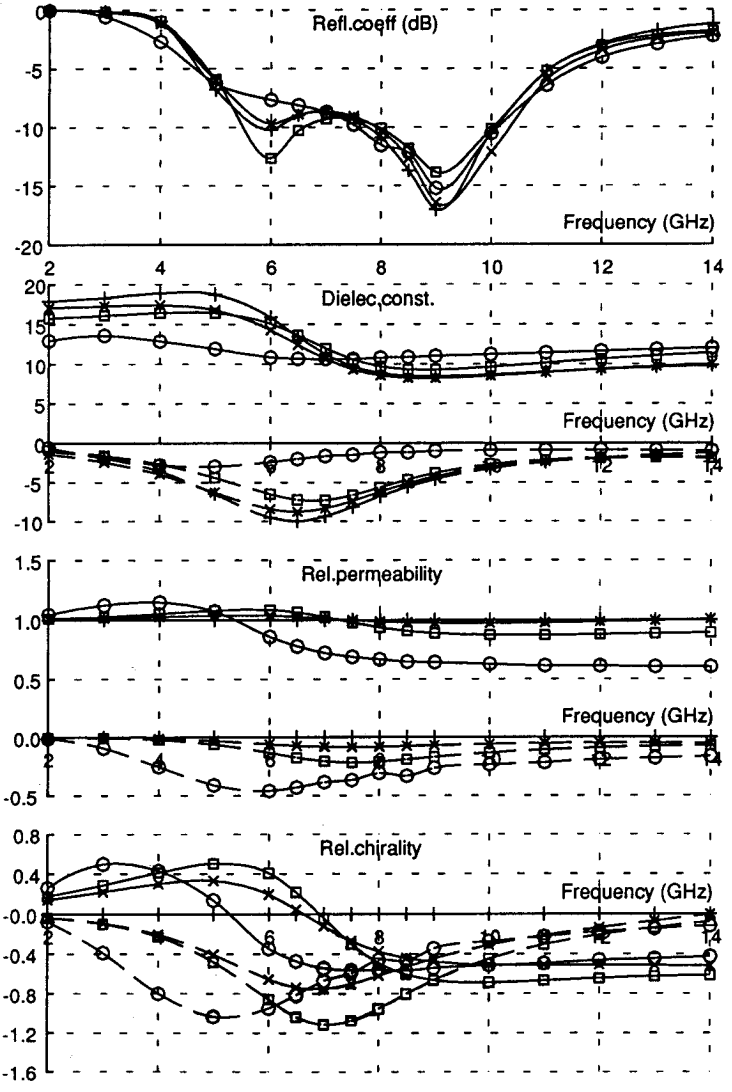

Figure 5 Reflection from layer of two-turn helices. $h/2r$: plus-infinity, cross= 2, square =1, 0=1/8, Full=real part, broken =image part.

of affecting reflection curve, and spiral and loops have nothing to offer that cannot be done with dipoles.

Just as one defines relative permittivity and permeability by dividing by ϵ_0 and μ_0 respectively, I define a relative chirality by dividing the chirality χ obtained from Eq. 11 by $\sqrt{\epsilon_0 \mu_0}$. The relative chirality values so obtained in these runs are comparatively small: for the one-turn spiral they do not exceed 0.4 in magnitude, and for the two- and four-turn spiral they do not exceed 1.5. Since the dielectric constant of these composites is typically in the range from 10 to 15, the chiral terms will be small compared to the dielectric effects. In the flatter spiral, the composite dielectric constant has a large contribution from the electric moment of the helices themselves, in addition to the dielectric constant of the host medium. Thus the spiral are more important as contributors to the dielectric constant than as chiral objects, and the introduction of chirality brings with it an overriding dielectric effect. Optimizations have also been performed with thicker layers, which produce lower dielectric constant media, but the dielectric effect of the spiral still dominates the chiral effect.

In summary, it appears that the chiral moments available from spiral are comparatively small compared to the electric moments inevitably introduced at the same time. The effect on the reflection coefficient is then dominated by the frequency dependence of the composite dielectric constant, and there is no sign that the chirality has any improvement to offer.

6. Conclusion

In this paper we have investigated the usefulness of chirality for improving the performance of radar absorbers. We obtained an algebraic formula for the reflection coefficient at normal incidence from a metal-backed chiral absorbing layer. The cross-polar reflection was zero, as could be shown from reciprocity. The chirality disappeared from the co-polar reflection result, suggesting that chirality was irrelevant to absorber performance. The apparent discrepancy with other published work is resolved on realizing that that work used a different definition of the chiral parameter, which is not directly equivalent to the one used here.

In practice any method of making a chiral medium will affect all the medium parameters, dielectric, magnetic and chiral, together. Thus to investigate what is possible one must start from a detailed analysis of the basic chiral objects. We then include all the effects of the actually available adjustable parameters, rather than varying a chirality which cannot be independently adjusted. We here performed such an analysis for a chiral composite medium containing resistive wire helices. The electric, magnetic, and chiral moments of the helices are computed, and these are used to find the properties of the composite medium, and hence the reflection coefficient of an absorbing layer. This process was then put under an optimization routine, which adjusts the parameters of the helices and host medium to minimize the reflection integrated over a band of frequencies. It was found that the shape of the reflection curve is not much affected by the aspect ratio of the included helices, including the non-chiral extremes cases of a straight wire and a flat loop. Thus by this test the introduction of chirality by wire helices has not yielded any improvement. The chirality is in all cases fairly small compared to the additional dielectric constant simultaneously introduced by the spiral.

References

1. Varadan, V. K., V. V. Varadan, and A. Lakhtakia, "On the possibility of designing anti-reflection coatings using chiral composites," *Journal of Wave-material Interaction*, Vol. 2 No. 1, 71–81, Jan 1987.
2. Jaggard, D. L., and N. Engheta, "Chirosorb as an invisible medium," *Elec. Lett.*, Vol. 25, No. 3, 173–174, 2 Feb 1989.
3. Jaggard, D. L., N. Engheta, and J. Liu, "Chiroshield: a Salisbury/Dallenbach alternative," *Elec. Lett.*, Vol. 26 No. 17, 1332–1334, 16 Aug 1990.
4. Jaggard, D. L., J. C. Liu, and X. Sun, "Spherical chiroshield," *Elec. Lett.*, Vol. 27, No. 1, 77–79, 3 Jan 1991.
5. Jaggard, D. L., A. R. Mickelson, and C. H. Papas, "On electromagnetic waves in chiral media," *Appl. Phys.*, Vol. 18, 211–216, 1979.
6. Varadan, V. V., A. Lakhtakia, and V. K. Varadan, "Equivalent dipole moments of helical arrangements of small, isotropic, point-polarizable scatterers: Application to chiral polymer design," *J. Appl. Phys.*, Vol. 63, No. 2, 280–328, Jan 1988.

7. Guire, T., V. V. Varadan, and V. K. Varadan, "Influence of chirality on the reflection of EM waves by planar dielectric slabs," *IEEE Trans EMC*, Vol. 32, 300–303, 1990.
8. Ro, R., V. V. Varadan, and V. K. Varadan, "Electromagnetic activity and absorption in microwave chiral composites," *IEE Proc. H*, Vol. 139, No. 5, 441–448, Oct 1992.
9. Umari, M. H., V. V. Varadan, and V. K. Varadan, "Rotation and dichroism associated with microwave propagation in chiral composite samples," *Radio Sci.*, Vol. 26, No. 5, 1327–1334, Sept 1991.
10. Hollinger, R. D, V. V. Varadan, D. K. Ghodgaonkar, and V. K. Varadan, "Experimental characterisation of isotropic chiral composites in circular waveguides," *Radio Sci.*, Vol. 27, No. 2, 161–168, March 1992.
11. Lakhtakia, A., V. K. Varadan, and V. V. Varadan, "Time-harmonic electromagnetic fields in chiral media," *Springer-Verlag Lecture Notes in Physics*, No. 355, Berlin, 1989.
12. Sihvola, A. H., and I. V. Lindell, "Bi-isotropic constitutive relations," *Microw. Opt. Technol. Lett.*, Vol. 4, No. 8, 295–297, July 1991.
13. Sihvola, A. H., and I. V. Lindell, "Chiral Maxwell-Garnet mixing formula," *Elec. Lett.*, Vol. 26 No. 2, 118–9, 18 Jan 1990.
14. Tretyakov, S A., et al., "Conductor backed Tellegen slab as a twist polarizer," *Elec. Lett.*, Vol. 28, No. 3, 281–282, 30 Jan 1992.
15. Burke, G. J., et al., "Numerical Electromagnetic Code (NEC) – Method of Moments," Technical document 116, Lawrence Livermore Laboratory, 1977.
16. Lindman, K. F., *Ann. Phys.*, Vol. 63, 621, 1920.
17. Lindman, K F., *Ann. Phys.*, Vol. 69, 270, 1922.
18. Tinoco, I., and M. P. Freeman, "The optical activity of oriented copper helices, I: experimental," *J. Chem. Phys.*, Vol. 61, 1196–1200, 1957.